CRYSTAL GROWTH & DESIGN

pubs.acs.org/crystal

Article

Formation of Strontianite and Witherite Cohesive Layers on Calcite Surfaces for Building Stone Conservation

Pablo Forjanes,* Carlos Pérez-Garrido, Pedro Álvarez-Lloret, José Manuel Astilleros, and Lurdes Fernández-Díaz*

Cite This: *Cryst. Growth Des.* 2022, 22, 6418−6428

Read Online

ACCESS | Metrics & More | Article Recommendations | Supporting Information

ABSTRACT: The formation of micrometric-thick mineral cohesive layers is a novel method to prevent the deterioration of historical buildings. Here, we study the formation of thin, cohesive, pseudomorphic shells of strontianite ($SrCO_3$) and witherite ($BaCO_3$) on the surface of calcite ($CaCO_3$) single crystals reacted with aqueous solutions bearing Sr^{2+} and Ba^{2+}, respectively. The reaction front moves inward from the calcite−solution interface through a dissolution−crystallization reaction, which stops before the strontianite and witherite shells are barely 40 thick. These shells consist of elongated crystallites that grow oriented on the calcite substrate, with which they share very small contact areas. The calcite−strontianite and −witherite epitaxies are mono-dimensional and involve a parallelism between $(10\bar{1}4)_{Cal}||(021)_{Str/Wth}$. Strontianite and witherite cohesive layers remain strongly attached to the calcite substrates, which appear crack-free even after 2 years of reaction time. The formation of thin, cohesive, and durable replacement layers of strontianite and witherite may provide a long-lasting protection for calcitic marbles and limestones used as building stones in cultural heritage.

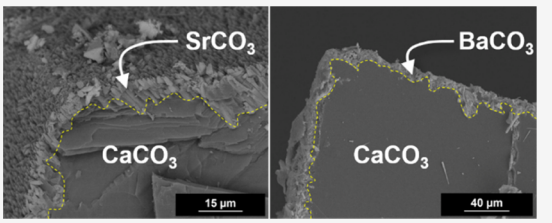

INTRODUCTION

Calcite is the stable polymorph of $CaCO_3$ under Earth surface conditions.[1] Moreover, calcite is the main mineral constituent of limestones and a major component of most marbles. Both limestone and marble are considered ornamental rocks and have been widely used as building materials since ancient times. Numerous cultural heritage buildings and structures are partially or entirely built with these rocks, from the Megalithic temples of Malta (Globigerine limestone) and the Greek Parthenon (Pentelic marble) to the Taj Mahal (Makrana marble) and many european royal palaces like those of Madrid and Aranjuez (Colmenar limestone). Most limestones and many marbles contain substantial volumes of porosity.[2] The presence of this porosity makes limestones and marbles highly prone to alteration as it provides them with large surface areas where the interaction with the environmental elements and colonization by microorganisms can take place.[3,4] An increasing awareness of the unique value of cultural heritage and the importance of preserving it for future generations has prompted the search of novel methods to prevent the deterioration of art treasures and historical buildings.[5,6] In the case of the latter, numerous treatments have been applied to prevent the alteration of building stones. One of these treatments consists of promoting the formation of mineral cohesive layers on the surfaces of the mineral grains that constitute the outermost external layers of the building stones.[3,5,7,8] These cohesive layers reduce the porosity of the building stones and, as a result, its exposure to potential alteration vectors (microorganisms, pollution, and acid atmospheres). This type of treatment has been successfully applied, both in situ and in the laboratory, to calcite crystals, on whose surface a micrometric thick layer is replaced by a cohesive layer of calcium oxalate after interaction with oxalate-bearing fluids.[5,6,9,10] Due to the large positive molar volume change (more than 50%) associated to this mineral replacement reaction, the so-formed calcium oxalate cohesive layer effectively protects the calcite substrates since it is virtually devoid of porosity.

A good adhesion between the substrate and the overgrowing cohesive layer is a key factor that determines how effectively the cohesive layer can preserve the building stone from alteration.[5,6,9] Indeed, the fragility of calcium oxalate cohesive layers and their proneness to detach from the calcitic substrates constitutes the main problem of this building stone treatment. Commonly, the existence of crystallographic relationships between the overgrowth and the substrate facilitates the formation of more strongly attached and less fragile overgrowths.[11−13] However, epitactic overgrown cohesive layers can also develop cracks due to accumulated tensile stress.[14−16] Though these cracks originate within the cohesive layer, they can often also penetrate the substrate, irreversibly damaging it

Received: April 1, 2022
Revised: September 3, 2022
Published: September 21, 2022

https://doi.org/10.1021/acs.cgd.2c00383
Cryst. Growth Des. 2022, 22, 6418−6428

and making its interior accessible to alteration vectors that can further increase the damage.[16] Therefore, the formation of cracks may become a major hindrance to the extended application of cohesive layer-based methods in the conservation of cultural heritage building stones.

Strontianite ($SrCO_3$) and witherite ($BaCO_3$) are orthorhombic carbonates (space group *Pmcn*; strontianite: a = 5.090 Å, b = 8.358 Å, and c = 5.997 Å; witherite: a = 5.3126 Å, b = 8.8958 Å, and c = 6.4284 Å), isostructural with aragonite ($CaCO_3$),[17] whereas calcite is trigonal (space group $R\bar{3}c$, a = 4.988 Å, and c = 17.061 Å).[18] Aragonite and calcite type structures share structural features since both consist of layers of hexagonally arranged calcium atoms alternating with also hexagonally arranged CO_3 layers.[19] The similarities between both types of structures increase the possibility for the development of epitactic relationships between crystals with aragonite-type and calcite-type structures.[20−22] Strontianite and witherite have molar volumes that are 5.6 and 24.1% larger than the molar volume of calcite, respectively. Therefore, we hypothesize that the replacement of a micrometric outermost layer of the calcite crystals by either strontianite or witherite may result in the formation of cohesive layers, constituting a potentially effective treatment for protecting limestone and marble surfaces from interaction with the alteration vectors.

In this work, we study the reaction of rhombohedral calcite single crystals with aqueous solutions that bear different Sr or Ba concentrations. The interaction results in the formation of strontianite or witherite replacement layers on the calcite substrates. By using a combination of different microanalytical techniques, we assess the existence of crystallographic relationships between the overgrown layers and the substrate. Furthermore, we investigate the influence of temperature, interaction time, and aqueous solution concentration in the textural and compositional features of the strontianite and witherite cohesive layers and evaluate the effect that the formation of these overgrowths may have on the calcite parent substrate. These results provide insights into the factors that must be considered when designing effective cohesive layer formation-based treatments for the protection of limestone and marble cultural heritage buildings.

EXPERIMENTAL SECTION

Several experiments of interaction were conducted between aqueous solutions bearing different concentrations of either Sr or Ba (0.05 and 1 M) and rhombohedral calcite surfaces. The aqueous solutions were prepared by dissolving reagent grade $SrCl_2{\cdot}6H_2O$ or $BaCl_2{\cdot}2H_2O$ (Sigma-Aldrich, St. Louis, MO, USA) in high-purity deionized water (Milli-Q; Burlington, MA, USA) (18 MΩ·cm). Highly pure optically clear calcite single crystals (Iceland spar variety) from Naica (Mexico) were used as starting material. These crystals were cleaved along the $(10\bar{1}4)$ planes in fragments of approximately 2 × 3 × 3 mm, which were then washed with deionized water and ultrasonically cleaned. For each experiment, three different calcite fragments were used.

Two types of experiments were performed: (1) experiments at 25 ± 0.5 °C and atmospheric pressure were performed in a thermostatic chamber (JP Selecta) by placing a calcite fragment together with 1.5 mL of aqueous solution in polypropylene reactors sealed with a lid. (2) Hydrothermal experiments at 70 ± 1.5 and 120 ± 5 °C under endogenous pressure were carried out by placing 3 calcite fragments into sealed polytetrafluorethylene liners filled with 4.5 mL of the aqueous solutions. The liners were placed in sealed stainless-steel autoclave reactors, and then, these were placed in a preheated oven (Memmert GmbH UN110 Single).

The experimental runs lasted between 30 min and 2 years (Table S1). Once the experiments were concluded, reactors were removed from either the thermostatic chamber or the oven, cooled to room temperature if required, and then opened. The interacted calcite fragments were removed from the solution, washed, first with Milli-Q water and then with ethanol, and left to dry overnight at 50 °C in the thermostatic chamber.

Molecular scale information on the early stages of the interaction between a Sr- or Ba-bearing aqueous solutions and calcite $\{10\bar{1}4\}$ was obtained by conducting in situ atomic force microscopy (AFM) experiments in contact mode at room temperature in the fluid cell of the Digital Instruments Multimode Nanoscope III (Bruker). Solutions with different Sr or Ba concentrations were used (0.001, 0.005, 0.01, 0.05, and 1 M). Calcite substrates were scanned with Silicon nitride (Si_3N_4) tips (Veeco NP-S10) with a nominal force constant of k = 0.06−0.58 N/m. The solution was kept static in the AFM fluid cell, and the interaction process was monitored by taking images at intervals of 50−60s. Massive nucleation of three-dimensional (3D) nuclei taking place in the bulk solution few seconds after the beginning of the experiments made it impossible to carry out AFM imaging using the 1 M aqueous solutions. In the case of experiments conducted with solutions containing Sr or Ba concentrations below 0.05 M, no nuclei formation was observed after ∼1 h interaction.

Reacted calcite samples were studied by scanning electron microscopy (SEM) and X-ray diffraction (XRD) analyses. The surfaces and cross sections of the reacted calcite crystals were imaged using the JEOL JSM 6400 and JEOL JSM 6335 scanning electron microscopes equipped with the Oxford Instruments 80 mm^2 X-Max SDD and Oxford Instruments 20 mm^2 energy dispersive spectrometers (EDX), respectively. The reacted calcite samples were mounted on holders and coated, first with carbon (Quorum Q150T-E; 8 nm) and then with gold (Quorum Q150R-S; 15 nm). Moreover, reacted calcite samples from 180 days long experimental runs were embedded in the epoxy resin (Struers) and then polished down to the middle parallel to $\{10\bar{1}4\}$, prior to being SEM imaged. Reacted calcite surfaces were imaged using secondary electrons (SE), while the cross sections were imaged using backscattered electrons (BSE).

Reacted calcite samples were further characterized by grazing incidence XRD (GIXRD) and powder XRD (PXRD). GIXRD diffractograms were collected using a PANalytical X'Pert PRO MRD with an angle of incidence of 0.1° on reacted calcite $\{10\bar{1}4\}$ surfaces in order to minimize the presence of peaks coming from the bulk calcite crystal. PXRD diffractograms were recorded from crushed reacted calcite samples with a microprocessor-controlled PANalytical X'Pert PRO MPD diffractometer, using a Cu Kα radiation source. Phase composition evaluation of the reacted samples was conducted by comparing the diffractograms to standard mineral files compiled in the crystallographic open database (COD, 2017 version) using the X'Pert and Match! Softwares. Furthermore, Rietveld refinement analysis was performed with the EdPCR program of the FullProf Suite (version 2.00)[23] and using the COD IDs 5000093 for strontianite,[17] 1000033 for witherite,[17] and 9000965 for calcite[18] as references to yield a semiquantitative estimation of the percentage of each mineral phase in the reacted samples (Figure S1).

Textural information on the reacted calcite samples was obtained from the analysis of bidimensional XRD (2D-XRD) patterns recorded using an X-ray diffractometer (Bruker D8 VENTURE) equipped with a CMOS area detector (PHOTON 100). The working conditions were set at 50 kV and 30 mA, using a Cu Kα source (λ = 1.54056 Å), with a pinhole collimator of 0.5 mm in diameter. The 2D-XRD patterns were registered by reflection mode, while rotating the sample 360° around the Φ angle (5° per step) with an acquisition time of 10 s per frame, setting the diffractometer ω and 2θ angles at 10 and 20°, respectively. The 2D-XRD frames were integrated in a one-dimensional pattern, and the pole figures (PF) at specific (hkl) crystallographic planes representing the 3D calcite (rhombohedral surface), strontianite, and witherite orientation were calculated using the XRD2DScan software.[24]

https://doi.org/10.1021/acs.cgd.2c00383
Cryst. Growth Des. 2022, 22, 6418−6428

RESULTS

Calcite Interaction with Sr-Bearing Aqueous Solutions. *AFM Observations.* As soon as the 0.05 M Sr-bearing aqueous solution is injected into the AFM fluid cell, rhombus-shaped etch pits nucleate on the calcite surfaces. These pits are similar to those observed during the interaction of calcite with deionized water (dashed line in Figure S2).[25,26] Calcite dissolution progresses through the retreat of monolayer cleavage steps and etch pit edges. The retreat accelerates ~40 min after the beginning of the interaction, concomitant to the formation of 3D nuclei of a new phase. The islands of the new phase show a slightly elongated shape and appear similarly oriented[25,27,28] (Figure 1).

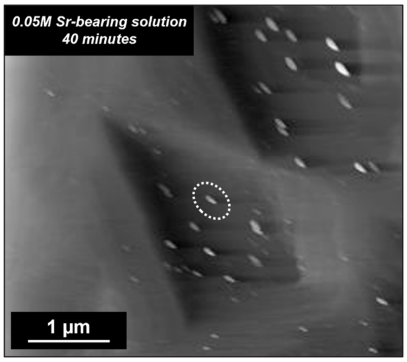

Figure 1. AFM image showing the oriented overgrowth of 3D nuclei (white dashed circle) on the $(10\bar{1}4)$ calcite surface after 40 min interaction with a 0.05 M Sr-bearing aqueous solution.

SEM imaging of calcite surfaces interacted with Sr-bearing aqueous solutions evidences the formation of new crystals that grow oriented on the calcite substrates (Figure 2a). These crystals are already clearly distinguishable on the surfaces of calcite samples reacted during 30 min, where they appear spatially associated to cleavage macro-steps on the calcite substrate (Figure 2a; yellow star). The density of new crystals on the flat terraces between macro-steps is very low (Figure 2a; blue star; Figure S3). As the interaction progresses, the new crystals progressively coalesce to build up tightly packed layers (Figure 2b). These layers completely carpet the calcite substrates after interaction times that decrease with increasing reaction temperature and Sr concentration in the aqueous solution (Table S2). GIXRD analyses confirm the overgrown layers as consisting of strontianite (Figure S4).

EDX analyses of the strontianite layers show that they contain Ca. The average Ca content of the strontianite crystals is 10.6 (±3.84) mole percent $CaCO_3$. No major differences in the Ca content of the strontianite crystals are observed as a function of temperature, interaction time, or Sr concentration in the aqueous solution (Figures S5−S11).

SEM images of cross-sections show that strontianite forms a thin layer around an unreacted calcite core. Table S2 summarizes the thickness of the strontianite rims that envelop calcite crystals reacted with 0.05 or 1 M Sr-bearing solutions at different temperatures during 30 days. In all the cases, the rims are less than 40 μm thick (Figure 3 and Table S2). The thickness of the overgrowth hardly increases after two years of interaction with the aqueous solution (Figure S12).

The results of PXRD Rietveld analysis (Figure S13) indicate that in all the reacted samples, strontianite represents less than 3.5 wt %, in agreement with the very small thickness of the strontianite layers, as observed in SEM micrographs.

High-resolution SEM images show that the strontianite layers consist of pseudohexagonal prismatic crystals that are elongated along the *c* axis and show marked re-entrant edges (Figure 4a). The presence of re-entrant edges is indicative of twinning. Thus, the pseudohexagonal habit is the consequence of the cyclic twinning characteristic of aragonite-type carbonate crystals, which involves three individual crystals joined by {110} planes (Figure 4a). Each individual crystal is bounded by the {110} and {010} prisms, with less developed faces that belong to the {111} rhombic bipyramid and the {021} prism. Strontianite crystals become more elongated, showing a more marked tapering with increasing temperature (Figure 4b). The Sr concentration in the aqueous solution also influences some morphological characteristics of strontianite crystals in the cohesive layers. Thus, crystals grown in contact with 0.05 M Sr aqueous solutions are larger (10−15 μm) than those formed from a 1 M Sr aqueous solutions (1−2 μm), where they often appear as spherulites (Figure S14)

Strontianite crystals grow oriented on the calcite substrates (Figure S15), though the orientation is poorer when the Sr concentration in the aqueous solution is 1 M (Figure S15d) or when the interaction time increases. 2D-XRD analyses were performed in order to determine the 3D orientation relationships between the strontianite overgrowth and the calcite

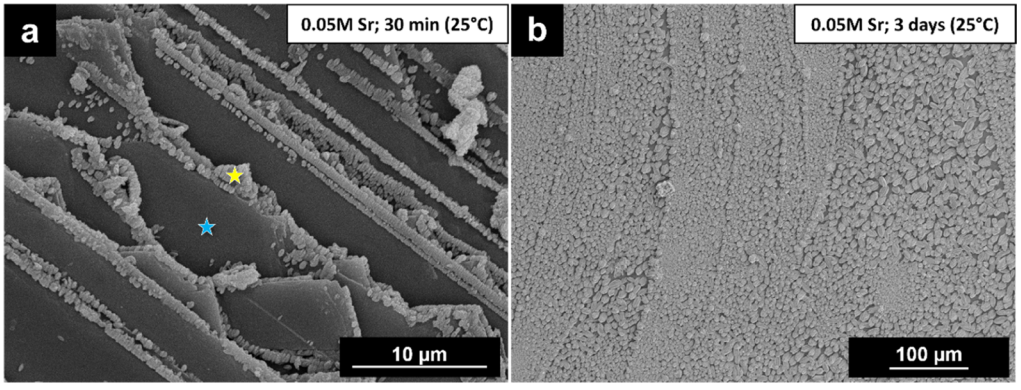

Figure 2. Interaction of calcite crystals with aqueous solutions bearing Sr leads to the formation of strontianite patches. (a) The secondary phase nucleates mostly at or closer to the original calcite exfoliation steps (yellow star). Contrarily, flat areas remain uncarpeted for longer times (blue star). (b) These patches later grow to constitute thick continuous layers.

https://doi.org/10.1021/acs.cgd.2c00383
Cryst. Growth Des. 2022, 22, 6418−6428

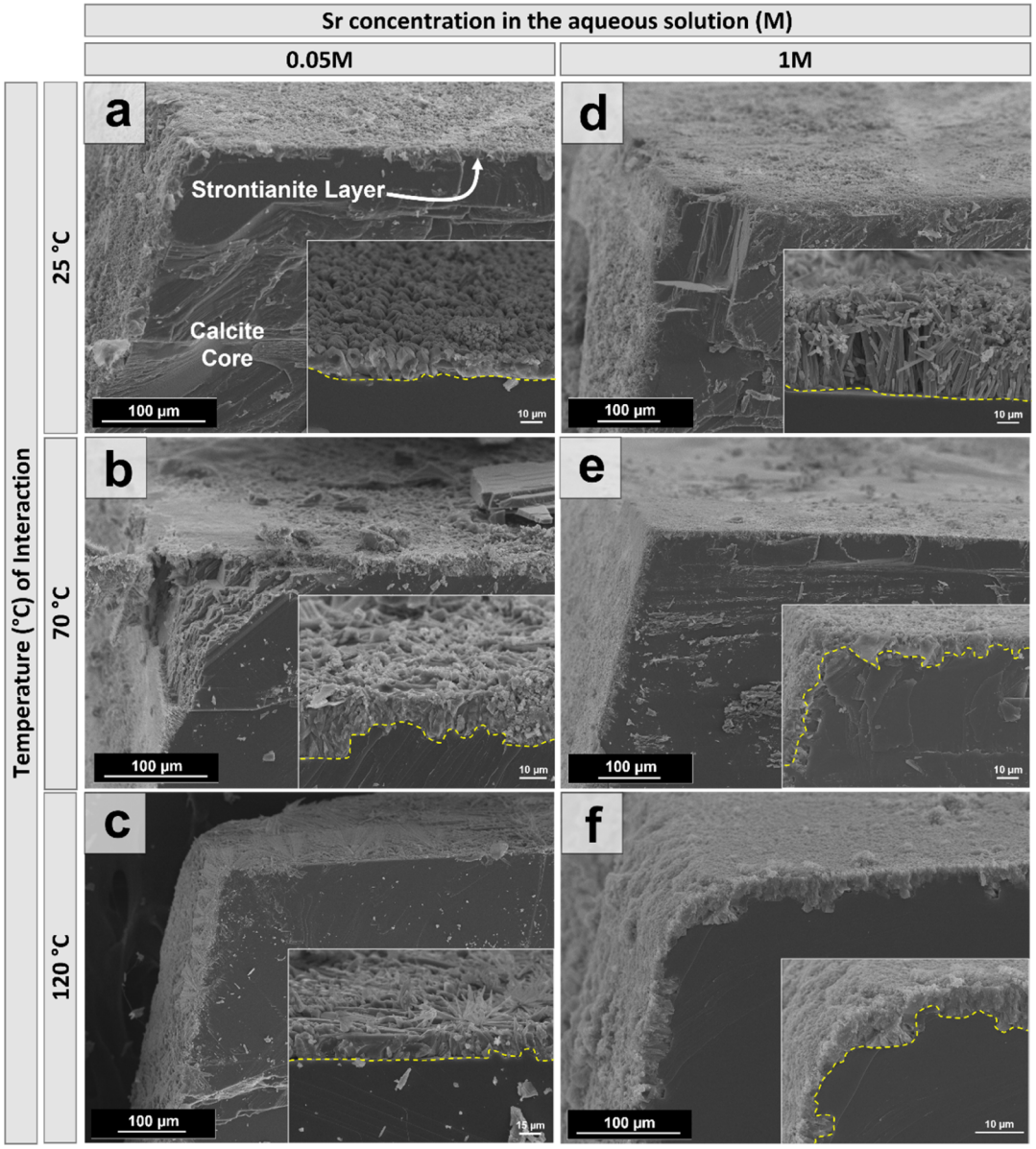

Figure 3. SEM images of cross-sections of calcite crystals after 30 days of interaction with Sr-bearing aqueous solutions. In all the cases, a thin strontianite layer encapsulates an unaltered calcite core. Regardless of the Sr concentration in the aqueous solution or the temperature of interaction, the strontianite cohesive layer is less than 40 μm thick.

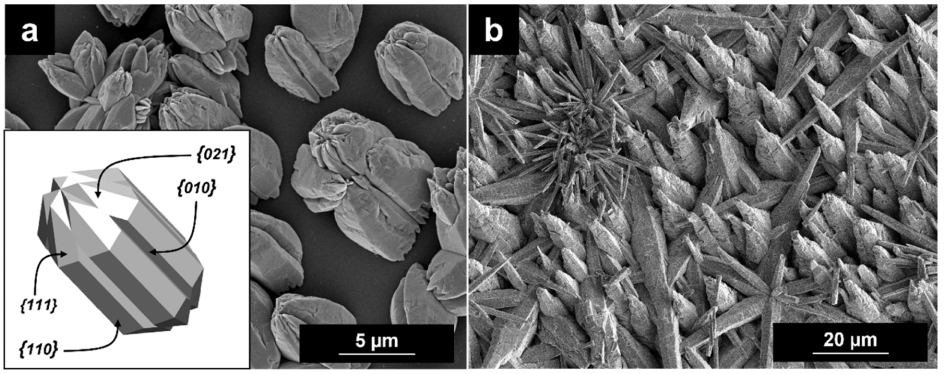

Figure 4. (a) SEM image of strontianite crystals growing on calcite $(10\bar{1}4)$ surfaces after interaction with a 0.05 M Sr-bearing aqueous solution at 25 °C. The crystals are twinned according to the aragonite law. The simulation of the twinned crystal was made using the software SHAPE, based on SEM observations. (b) SEM image of strontianite crystals formed upon interaction with a 0.05 M Sr-bearing aqueous solution at 70 °C.

https://doi.org/10.1021/acs.cgd.2c00383
Cryst. Growth Des. 2022, 22, 6418−6428

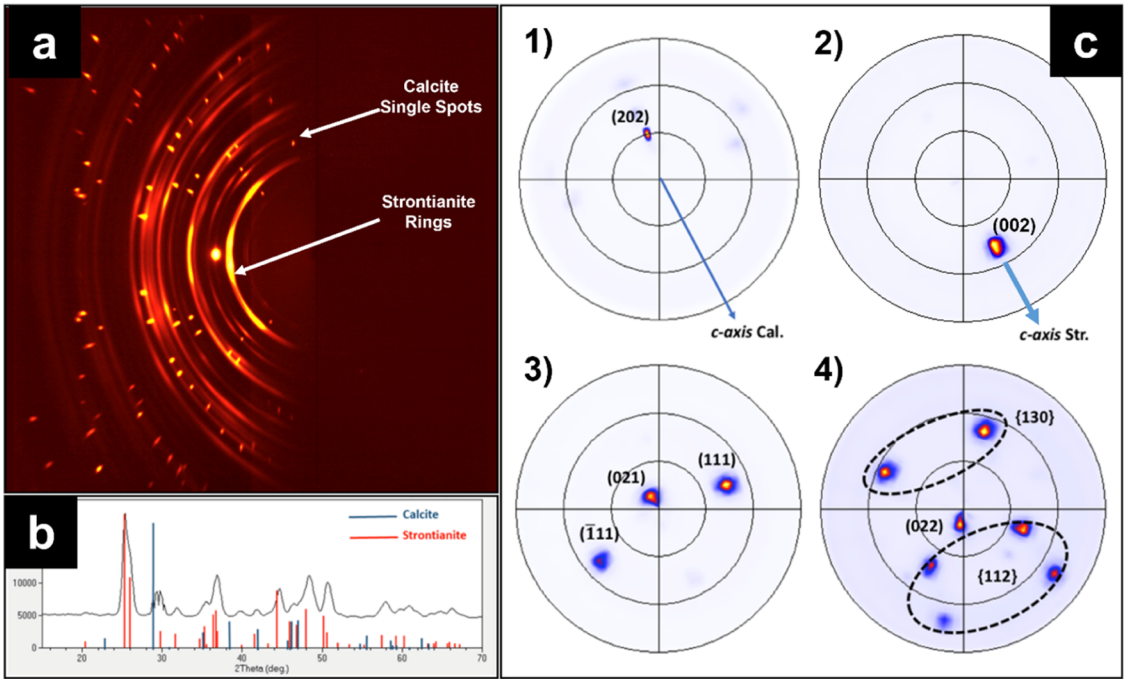

Figure 5. 2D-XRD analyses performed on calcite surfaces after 1 day interaction with a 0.05 M Sr-bearing aqueous solution at 120 °C. (a) 2D-XRD pattern (phi-rotation scan each 5° step, combination of superimposed 72 frames) from the calcite crystal surface (strong single crystal spots), together with strontianite overgrowth crystals (Debye−Scherrer diffraction rings). (b) 2θ scan profile obtained from the radial integration of the 2D-XRD pattern for calcite (blue lines) and strontianite (red lines) mineral phases. (c) PFs obtained from 2D-XRD analyses, showing the crystallographic relationships between the rhombohedral calcite surface and the overgrowing strontianite. (1) PF for (202) calcite reflection, tilted approximately 31° from the figure center. (2) PF for (002) strontianite reflection, showing a maximum titled approximately 55° from the figure center. (3) PF for the combined (021) + {111} strontianite reflections, displaying two maxima tilted approximately 47° from the PF center, (111) and ($\bar{1}$11) reflections and a maximum corresponding to the (021) orientation. (4) PF for the combined (022) + {130} + {112} reflections for strontianite crystals, confirming the preferential orientation for strontianite crystals.

substrate. The 2D-XRD patterns show the presence of well-defined and high-brilliance diffraction single spots, corresponding to the calcite substrate (i.e., coherently as a single crystal). Moreover, the 2D-XRD patterns also display different Debye−Scherrer diffraction rings (i.e., *hkl* reflections) associated to the polycrystalline strontianite overgrowth (Figure 5a). Superimposed on these diffraction rings, the intensity is concentrated in arcs, indicating that the overgrowth of strontianite shows a certain degree of preferential orientation. The preferential orientation of the strontianite crystals on calcite ($10\bar{1}4$) surfaces was further characterized by the determination of the PFs from several (*hkl*) reflections. These reflections were identified from the one-dimensional scan (i.e., 2θ diffraction pattern) obtained from the radial integration of the 2D-XRD patterns (Figure 5b). PFs corresponding to a calcite sample interacted with a Sr-bearing aqueous solution for 1 day and are shown in Figure 5c. The PF for calcite (202) reflection (Figure 5c; number 1), tilted approximately 31° from the figure center, indicates that the sample is oriented parallel to the calcite ($10\bar{1}4$) surface. For the strontianite overgrowth, the PF for the (002) reflection (Figure 5c, number 2) displays a maximum tilted approximately 55° from the figure center, indicating the strontianite *c*-axis direction. The combined PF for strontianite (021) reflection (Figure 5c, number 3) displays a maximum approximately at the center and two maxima for {111} reflections, tilted approximately 47° from the center. The combined PF for (022), {130}, and {112} strontianite reflections (Figure 5c, number 4) confirmed the preferential orientation of the strontianite crystals. Overall, these 2D-XRD analyses confirm the existence of a crystallographic orientational relationship between the calcite substrate and the strontianite overgrowth, defined by the parallelism between $(10\bar{1}4)_{Cal}$ and $(021)_{Str}$.

Calcite Interaction with Ba-Bearing Aqueous Solution. The interaction of calcite crystals with Ba-bearing aqueous solutions leads to the formation of oriented witherite cohesive layers that show similar characteristics to those described above for the strontianite overgrowth (Figure S16). However, the complete carpeting of the calcite substrates by witherite requires much longer interaction times than those needed for strontianite (Table S2). Furthermore, the witherite cohesive layers are slightly thinner than those of strontianite, with maximum average thickness ~25 μm (Figures 6 and S12).

The results of the Rietveld analysis derived from XRD data confirm that witherite accounts for less than 2.5 wt % in all the reacted samples, regardless of the Ba concentration, interaction time, and the temperature in the experiment (Figure S17).

Witherite cohesive layers consist of pseudohexagonal prismatic crystals that are bounded by the same faces and show similar tapering and identical twinning as the crystals that constitute the strontianite layers. The most remarkable morphological difference between witherite and strontianite crystals regards their size, which is significantly larger in the case of witherite. Thus, witherite crystals formed in contact with 0.05 M Ba bearing aqueous solutions show average sizes of around 25 μm, compared to the 10−15 μm size of strontianite crystals formed in contact with the equivalent counterpart solutions (Figure 7a). Witherite crystals grown in the 1 M aqueous solution appear mostly as spherulites (Figure 7b). EDX analyses indicate that witherite crystals incorporate

https://doi.org/10.1021/acs.cgd.2c00383
Cryst. Growth Des. 2022, 22, 6418−6428

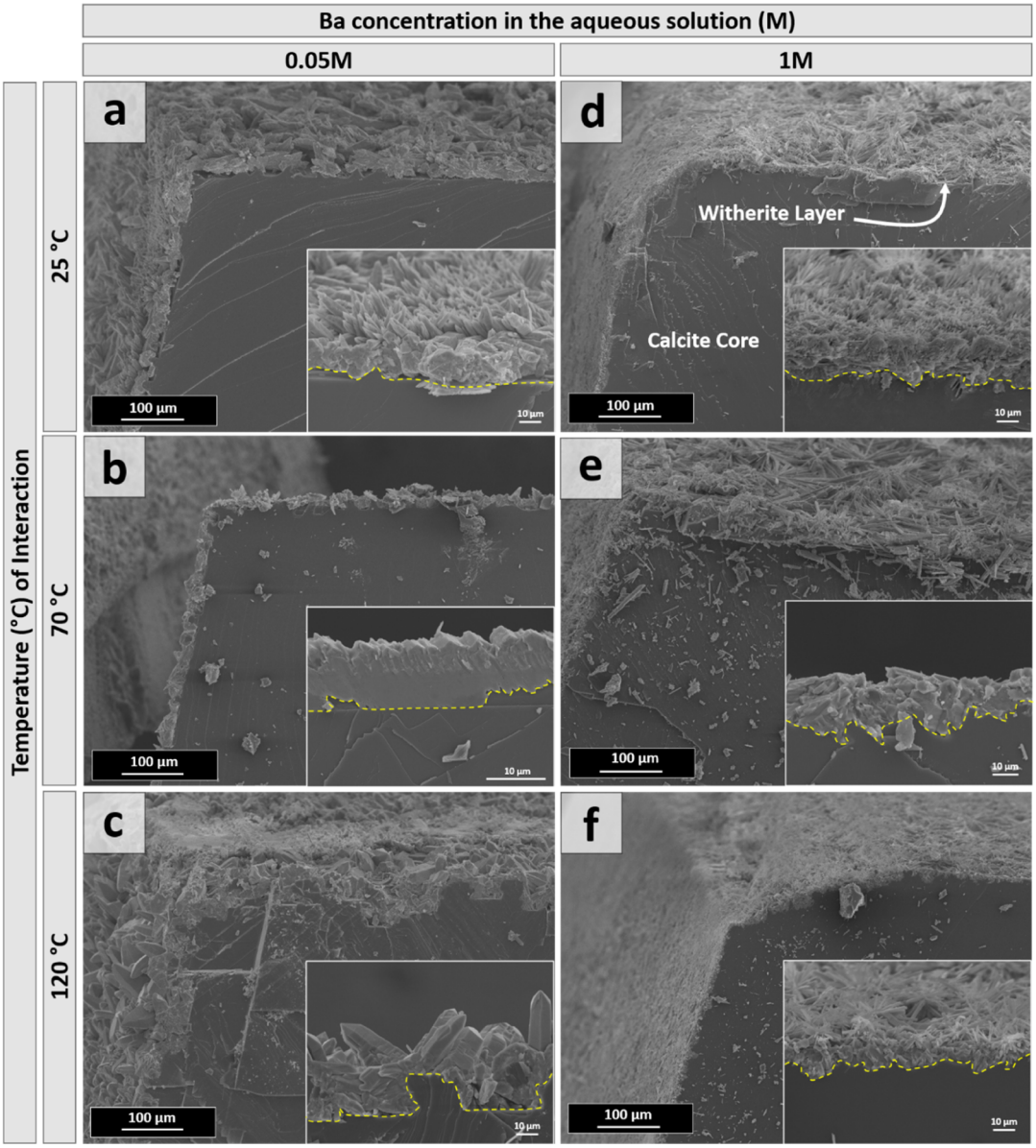

Figure 6. SEM images of cross-sections of calcite crystals after 30 days interaction with Ba-bearing aqueous solutions. In all the cases, a thin witherite layer encapsulates an unaltered calcite core. Regardless of the Ba concentration in the aqueous solution or the temperature of the interaction, the witherite cohesive layer is less than 25 μm thin.

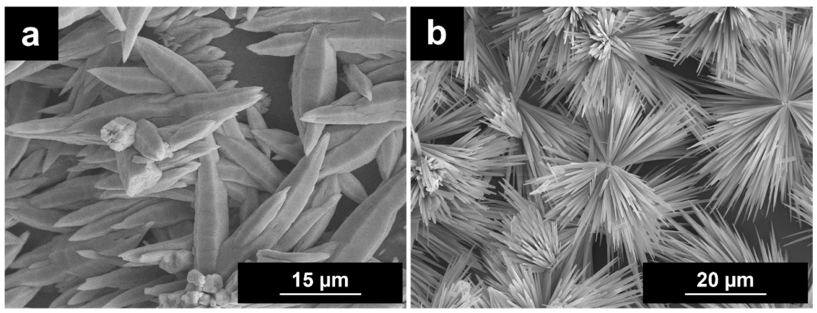

Figure 7. (a) SEM image of witherite crystals growing on calcite $(10\bar{1}4)$ surfaces after 7 days interaction with a 0.05 M Ba-bearing aqueous solution at 25 °C, showing the characteristic pseudohexagonal morphology. (b) Witherite growing on calcite $(10\bar{1}4)$ surfaces after 4 days interaction with a 1 M Ba-bearing aqueous solution.

lower amounts of Ca than strontianite crystals do [average Ca content of 4 (±2.65) mole percent $CaCO_3$] (Figures S5–S11).

Similar to that observed for strontianite crystals, witherite crystals grow oriented on calcite $(10\bar{1}4)$ surfaces. This orientation is apparent when witherite crystals form in contact

https://doi.org/10.1021/acs.cgd.2c00383
Cryst. Growth Des. 2022, 22, 6418−6428

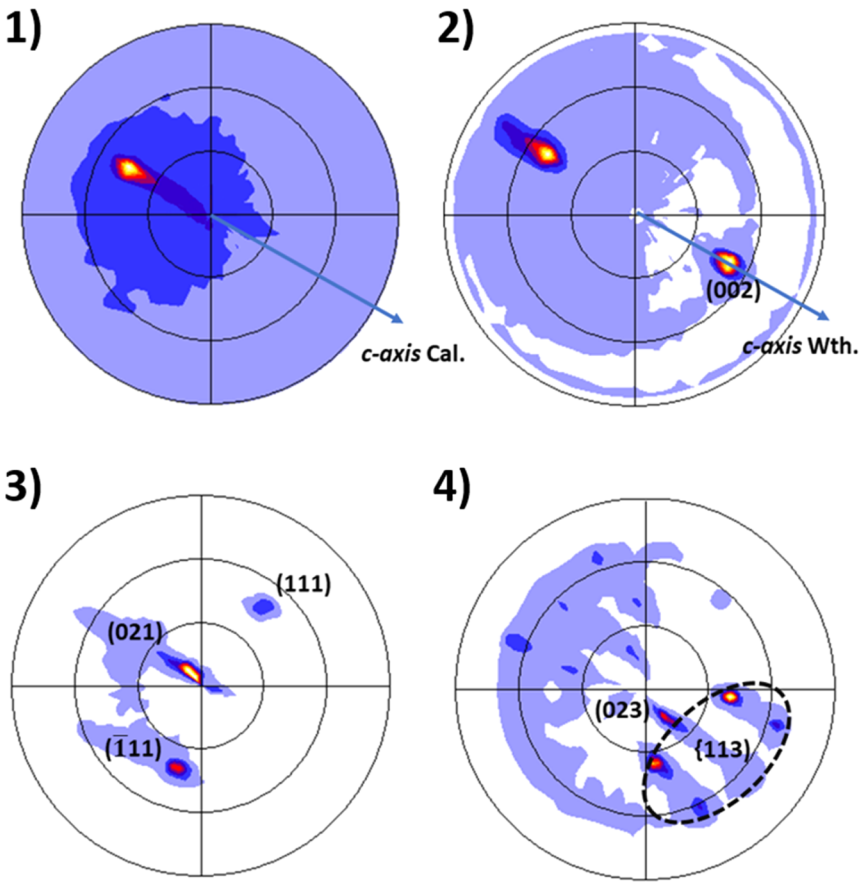

Figure 8. PFs obtained from 2D-XRD analyses, showing the crystallographic relationship between the calcite surface and the witherite overgrowth. The analyses were performed on calcite surfaces after 1 day interaction with a 0.05 M Ba-bearing aqueous solution at 120 °C. (1) PF for (006) calcite reflection tilted approximately 44° from the figure center, indicating the direction of the *c*-axis direction. (2) PF for (002) witherite reflection, showing two maxima titled approximately 55° from the figure center, indicating the direction of the *c*-axis. (3) PF for the combined (021) + {111} witherite reflections, displaying two maxima corresponding to the (111) and ($\bar{1}$11) reflections and a centered maximum corresponding to the (021) orientation. (4) PF for the combined (023) + {113} reflections, confirming the orientation of witherite replacement.

with 0.05 M Ba-bearing aqueous solutions (Figure S18a−c). However, it is not distinguishable in the case of witherite crystals that form in contact with 1 M Ba aqueous solutions as they grow as spherulites (Figure S18d). The preferential orientation observed in the witherite crystals overgrown on rhombohedral calcite surfaces in contact with 0.05 M Ba-bearing aqueous solution was characterized by 2D-XRD analyses. PFs describing the crystallographic relationships between calcite and witherite crystals are shown in Figure 8. As previously reported for the strontianite overgrowth, 2D-XRD analyses confirmed the crystallographic relationships between calcite and witherite as $(10\bar{1}4)_{Cal}||(021)_{Wth}$.

DISCUSSION

In contact with Sr or Ba-bearing aqueous solutions, the surface of calcite single crystals undergoes dissolution, releasing CO_3^{2-} and Ca^{2+} ions to the fluid. As a result, supersaturation with respect to strontianite or witherite rapidly mounts up until the threshold value for the heterogeneous nucleation of these phases is overcome.[29] At this point, strontianite or witherite nuclei form on the calcite substrate and, as they grow, remove CO_3^{2-} and Sr^{2+} or Ba^{2+} ions from the fluid. This promotes further dissolution of calcite, which in turn leads to additional strontianite or witherite precipitation. Soon after this feedback loop is defined, the rates of calcite dissolution and strontianite/witherite precipitation become tightly coupled. It could be expected that this dissolution−precipitation feedback loop should operate as long as undissolved calcite remained and the concentration of Sr^{2+} or Ba^{2+} in the fluid remained high enough to allow the precipitation of strontianite or witherite.[30] Contrarily, our results indicate that this dissolution−precipitation feedback loop is strikingly short lived. Regardless of the experimental conditions (temperature or Sr or Ba concentration in the aqueous solution), calcite crystal surfaces become passivated after the formation of thin (<40 μm) strontianite or witherite cohesive layers. Therefore, in both systems (calcite-strontianite; calcite-witherite), an identical outcome is achieved: the armoring of the calcite surface from further interaction with the fluid. However, specific features (thickness, size and co-orientation degree of constituting crystals, Ca content, etc.) of each type of replaced layer may influence its long-term adhesion to the calcite substrate. Both the strontianite and witherite replacement layers define shell-like rims surrounding unreacted calcite cores. These cohesive layers are strikingly resistant and remain well attached to the substrate after two years in contact with the aqueous phase. Furthermore, their prolonged interaction with the fluid does not result in major textural or compositional evolution (Figures S5−S11).

Two main factors contribute to the swiftness of the passivation of calcite surfaces by thin strontianite and witherite layers: (i) the development of an epitaxy involving the calcite

https://doi.org/10.1021/acs.cgd.2c00383
Cryst. Growth Des. 2022, 22, 6418−6428

substrate and both strontianite and witherite overgrowths and (ii) the molar volume change involved in the calcite dissolution-strontianite/witherite precipitation reaction.

As explained above, the strontianite and witherite crystals that constitute the overgrowths show habits bounded by the {111}, {021}, {110}, and {010} forms, the 4 most stable ones, as predicted by the Donnay Harker's rule for strontianite and witherite.[31] Both strontianite and witherite crystals show tapered faces, although the tapering is more marked in the former ones (Figures 4 and 7). The different degree of tapering between strontianite and witherite crystals can be explained by the incorporation of larger amounts of Ca in strontianite since the development of tapered surfaces has commonly been attributed to the effect of impurities adsorbed during growth.[32−34] The incorporation of Ca into the structures of strontianite and witherite can also explain the formation of spherulites at latter stages of the growth process. Due to the smaller size of Ca^{2+} (ratio Ca^{IX} = 1.18 Å) compared to Sr^{2+} (ratio Sr^{IX} = 1.31 Å) and, more so, Ba^{2+} (ratio Ba^{IX} = 1.47 Å), this incorporation induces strain in the lattice of both strontianite and witherite. This lattice strain can be released through the formation of dislocations. The arrangement of these dislocations at regular intervals will the result in the formation of small angle boundaries, giving rise to the split growth phenomenon and, eventually, to the formation of spherulites.

SEM imaging and 2D-XRD analysis evidence that strontianite and witherite (021) faces grow parallel to the calcite $(10\bar{1}4)$ substrates, that is, $(10\bar{1}4)_{Cal}||(021)_{Str/Wth}$.[35,36] This epitaxy can be characterized by considering the crystallographic matching between the substrate and overgrowth crystal structures along the [010] direction in calcite and the [100] direction in strontianite and witherite. The misfit between these directions can be calculated with the expression[37,38]

$$mf = \frac{t[uvw]_{\text{Str or Wth}} - t[uvw]_{\text{Cal}}}{t[uvw]_{\text{Cal}}}$$

where $t[uvw]$ is the Ca−Ca repeating period along the [010] direction for calcite (4.988 Å) and the Sr−Sr and Ba−Ba repeating period along the [100] direction in strontianite (5.090 Å) and witherite (5.313 Å). This calculation yields linear misfit values of 2.0 and 6.3% for the calcite−strontianite and the calcite−witherite structural matchings, respectively. Both values are clearly within the limits (≤|10−12%|) for the formation of an epitactic layer.[37,39] Furthermore, the defined matching involves a crystallographic relationship along directions that are parallel to periodic bond chains (PBCs) in the structures of both calcite and strontianite/witherite.[31] This scenario favors the oriented growth of strontianite or witherite on calcite as the coincidence between close-packed atomic rows minimizes the interface energy.[12,39] It is well established that the existence of epitactic relationships between the substrate and overgrowth can strongly influence the kinetics of solvent-mediated replacement reactions.[11,28,40−43] This influence is highest when the replacement involves isostructural phases that belong to the same mineral group. In such cases, structural misfits are commonly very low and epitactic overgrowths often form through the Frank-van der Merwe or the Stranski−Krastanov growth mechanisms[37,39] as epitactic 2D nuclei grow and coalesce to build up highly cohesive nanometric layers. The formation of these overgrowths rapidly armors the substrate and prevents its interaction with the bulk solution.[11,28,40,41,43−45] When solvent-mediated replacement reactions involve mineral phases with relatively poor structural matchings, the formation of epitactic replacing overgrowths is commonly governed by the Volmer−Weber mechanism. These overgrowths are less cohesive and show less rigorous epitactic relationships with the substrate than those formed through the Frank-van der Merwe or the Stranski−Krastanov mechanisms. Furthermore, they consist of 3D nuclei which form in inhomogeneities associated to the substrate and mainly grow out of the epitactic plane, with rather limited lateral growth on the substrate.[34] The matching between the structures of strontianite and witherite and the structure of calcite is good enough to allow the oriented nucleation and growth of the former phases on calcite $\{10\bar{1}4\}$ substrates. However, both epitaxies are mono-dimensional as they only involve the parallelism of just one crystallographic direction within the epitactic plane of each overgrowth-substrate pair: $[100]_{\text{Str or Wth}}//[010]_{\text{Cal}}$. It can be expected that such mono-dimensional epitactic overgrowths will form through the Volmer−Weber mechanism. Indeed, the results of in situ AFM experiments of the interaction between calcite $\{10\bar{1}4\}$ surfaces and Sr-bearing solutions and SEM observations support this interpretation as strontianite and witherite oriented 3D-nuclei appear associated to steps and dissolution pits (Figure 2a), and substrate inhomogeneities play a key role in the Volmer−Weber mechanism.[34] Furthermore, crystal morphological and textural features, as evidenced by SEM imaging, are also in good agreement with the Volmer−Weber mechanism governing the formation of strontianite and witherite overgrowths on calcite, especially during the early stages of the process. In both overgrowths, crystals first form decorating macro-steps on the calcite surface (Figure 2a). Individual crystallites are elongated out of the epitactic plane, with which they share very small contact areas, as expected for crystallites with limited lateral growth on the calcite substrate. The observation that as the replacement reaction progresses, the co-orientation between crystal individuals within the overgrowth decreases and the epitactic relationships between the overgrowth and substrate are progressively lost is also consistent with the Volmer−Weber mechanism.

The coexistence of several epitactic relationships within Volmer−Weber epitactic layers determines that these layers accumulate small amounts of porosity as differently oriented 3D nuclei coalesce and leave micropores trapped between them.[38,46] Epitactic overgrowth porosity plays a key role in guaranteeing the progress of solvent-mediated mineral replacement reactions. After the surfaces of the parent crystals become totally carpeted by a secondary phase epitactic overgrowth, the existence of a network of interconnected pores within the epitactic layer provides a path for the continuous communication between the primary−secondary phase interface and the bulk solution.[47,48] When the replacement reaction involves a negative molar volume change, the preservation of the external shape of the primary phase requires that the molar volume loss is balanced by the generation of an equal volume of transitional porosity.[30,49] This porosity adds up to the intrinsic characteristic of Volmer−Weber epitactic layers. The permeability of the resulting porosity network depends on a variety of features, including the total porosity volume, its size, morphology, density and distribution, its interconnectivity, and so

https://doi.org/10.1021/acs.cgd.2c00383
Cryst. Growth Des. 2022, 22, 6418−6428

forth.[46,48−50] Volmer−Weber layers that contain both intrinsic microporosity and porosity, generated as a result of the pseudomorphic mineral replacement reaction fail to effectively armor the underlaying substrate. Thus, the formation of such Volmer−Weber epitactic layers may significantly slowdown the kinetics of mineral replacement reactions but rarely preclude their progress.[5,46,48,50,51] Both strontianite and witherite have larger molar volumes than calcite (V_{Str} = 39.01 cm^3/mol, V_W = 45.81 cm^3/mol, V_{Cal} = 36.94 cm^3/mol). The molar volume increases involved in the calcite-by-strontianite (ΔV = + 2.07 cm^3/mol; +5.6%) and calcite-by-witherite (+8.87 cm^3/mol; +24.1%) replacement reactions determine the formation of very compact overgrowths which only contain a small volume of isolated micropores. The lack of interconnected porosity within these overgrowths makes them impermeable to the fluid, preventing significant mass transfer from the bulk fluid to the reactive interface between the Volmer−Weber replacement layer and the unaltered calcite core.[42,52−54] Slight differences in the molar volume change involved in both replacement reactions can result from differences in the amount of Ca incorporated into strontianite and witherite as this incorporation will contribute to the decrease of the molar volume of both phases. In any case, the impact of these differences on the textural features of the strontianite- and witherite-replaced layers will be very small and will not significantly affect the effectiveness of their armoring of the calcite surface.

Interestingly, there are numerous examples of dissolution−crystallization reactions that, despite involving significant positive molar volume changes and the formation of epitactic overgrowths, steadily progress to reach completion, with the primary phase being fully replaced by the secondary one.[14,15,55−57] In most of these cases, the progress of the reaction is promoted by the formation of cracks which originate at the substrate−overgrowth interface and propagate within the primary phase, defining a network of fractures. The replacement of the primary crystal takes place along fractures since they provide a path for the infiltration of the fluid phase. It has been interpreted that cracks form due to the stress generated by the increase in the molar volume.[14,58] Furthermore, it has been stated that the nucleation of crystals of the secondary phase on point and line defects of the primary phase surfaces generates stress-concentrating environments from where fracturing propagates, similarly as that observed during metal corrosion.[59−61] Surprisingly, despite the significant increase in the molar volume associated to the transformation of calcite into strontianite (+5.6%) and the very large one associated to its transformation into witherite (+24.1%), no cracks are observed in crosscut sections of calcite crystals partially replaced by either strontianite or witherite, even after 2 years interaction with the fluid. Gillet et al. (1987)[58] observed that during the pseudomorphic replacement of abiogenic aragonite by calcite, which involves a molar volume change of +8.4%, fracturing only occurred when calcite crystals in the overgrowth reached sizes well over 50 micrometres. As explained above, strontianite and witherite overgrowths consist of very small, elongated crystals that during the early stages of the replacement, grow approximately perpendicular to the calcite surface, sharing a very small area with the calcite substrate at the interface. This may determine that the stresses generated by the positive molar volume change involved in the calcite-by-strontianite and calcite-by-witherite replacement reactions are not large enough to trigger the fracturing of the calcite substrate. This could explain the effective passivation of calcite substrates by very thin strontianite and witherite overgrowths. The formation of small amounts of porosity that compensates the amount of the primary phase lost to the solution when this is replaced by a less soluble secondary phase may explain that the replacement of calcite-by-strontianite, a phase significantly less soluble than calcite, progresses further than the replacement of calcite-by-witherite, which is slightly less soluble than calcite.[30]

CONCLUSIONS

This study shows that the interaction of calcite single crystals with Sr- or Ba-bearing aqueous solutions leads to the formation of cohesive layers of strontianite and witherite, respectively, through a coupled dissolution−crystallization mechanism. These layers are composed of small, elongated crystals that grow oriented on the underlying calcite substrate. The reaction temperature and starting Sr or Ba concentration in the fluid influence the crystal size, habit, and composition of the strontianite and witherite crystals of the overgrowths. However, regardless of the experimental conditions, thin, micrometric cohesive overgrowths of strontianite and witherite invariably passivate the calcite crystals, which appear as unreacted, crack-free cores after reaction times as long as 2 years. We attribute the high effectiveness of the calcite surface armoring by strontianite and witherite overgrowths to their low porosity as both calcite-by-strontianite and calcite-by-witherite replacement reactions involve positive molar volume changes. Moreover, strontianite and witherite epitactic overgrowths form through the Volmer−Weber growth mechanism and consist of individual small crystallites which share very small contact areas with the calcite substrate. This explains the absence of stress-related fracturing, a phenomenon which is often observed in pseudomorphic replacement reactions involving positive molar volume changes. This absence of fractures and porosity prevents the infiltration of the bulk fluid to the calcite substrate and explains the effectiveness of calcite surface passivation by strontianite and witherite overgrowths.

Long-term experiments (over 2 years interaction) confirmed the absence of any fracturing signs in the calcite core and evidenced excellent overgrowth-substrate adherence as no overgrowth detachment was observed in any of the systems. These results support that the formation of strontianite and witherite cohesive layers could be incorporated in treatment protocols to prevent the alteration of building limestones and marbles in historic buildings as these overgrowths behave as strong and durable protective layers. The specific characteristics of strontianite and witherite cohesive layers (thickness, size and co-orientation degree of constituting crystals, Ca content, etc.) may influence their long-term adhesion to the calcite substrate. Qualifying this influence will require further research. Similarly, the formation of strontianite and witherite cohesive layers in calcite-bearing polycrystalline materials like marbles and limestones may show characteristics that differ from those observed for calcite single crystals since the existence of grain boundaries and differently oriented calcite crystal surfaces may facilitate fluid infiltration and the development of different epitactic relationships. This issue also needs to be addressed in future research. The results from this work also help to explain the scarcity of natural strontianite or witherite deposits linked to the replacement of calcium carbonates.

https://doi.org/10.1021/acs.cgd.2c00383
Cryst. Growth Des. 2022, 22, 6418−6428

■ ASSOCIATED CONTENT

Supporting Information

The Supporting Information is available free of charge at https://pubs.acs.org/doi/10.1021/acs.cgd.2c00383.

Supporting Information is available for this work. Additional details of the experimental procedure and an extension of SEM, EDX, XRD, and AFM results which are not included in the main text; and qualitative data regarding features of the strontianite/witherite replaced layer (PDF)

■ AUTHOR INFORMATION

Corresponding Authors

Pablo Forjanes − *Department of Mineralogy and Petrology, Complutense University of Madrid, 28040 Madrid, Spain;* orcid.org/0000-0003-4043-0788; Email: pforjane@ucm.es

Lurdes Fernández-Díaz − *Department of Mineralogy and Petrology, Complutense University of Madrid, 28040 Madrid, Spain; Instituto de Geociencias (IGEO), (UCM, CSIC), 28040 Madrid, Spain*; Email: lfdiaz@geo.ucm.es

Authors

Carlos Pérez-Garrido − *Department of Mineralogy and Petrology, Complutense University of Madrid, 28040 Madrid, Spain*

Pedro Álvarez-Lloret − *Department of Geology, Faculty of Geology, University of Oviedo, 33005 Oviedo, Spain;* orcid.org/0000-0001-5325-183X

José Manuel Astilleros − *Instituto de Geociencias (IGEO), (UCM, CSIC), 28040 Madrid, Spain*

Complete contact information is available at: https://pubs.acs.org/10.1021/acs.cgd.2c00383

Notes

The authors declare no competing financial interest.

■ ACKNOWLEDGMENTS

P.F. acknowledges a FPU Predoctoral contract (FPU17/01689). This study was supported by the Spanish MINECO under the projects CGL2016-77138-C2-1-P; PID2021-125467NB-I00; and PCI2019-111931-2. The authors thank the National Centre of Electronic Microscopy (CNME) and the X-ray CAI of the Complutense University of Madrid for kindly providing technical support to their research.

■ REFERENCES

(1) Morse, J. W.; Arvidson, R. S.; Lüttge, A. Calcium carbonate formation and dissolution. *Chem. Rev.* **2007**, *107*, 342−381.

(2) Sassoni, E.; Franzoni, E. Influence of porosity on artificial deterioration of marble and limestone by heating. *Appl. Phys. A* **2014**, *115*, 809−816.

(3) Maravelaki-Kalaitzaki, P. Black crusts and patinas on Pentelic marble from the Parthenon and Erechtheum (Acropolis, Athens): Characterization and origin. *Anal. Chim. Acta* **2005**, *532*, 187−198.

(4) Hällström, J.; Barup, K.; Grönlund, R.; Johansson, A.; Svanberg, S.; Palombi, L.; Lognoli, D.; Raimondi, V.; Cecchi, G.; Conti, C. Documentation of soiled and biodeteriorated facades: A case study on the Coliseum, Rome, using hyperspectral imaging fluorescence lidars. *J. Cult. Herit.* **2009**, *10*, 106−115.

(5) Ruiz-Agudo, E.; Putnis, C. V. Direct observations of mineral fluid reactions using atomic force microscopy: The specific example of calcite. *Mineral. Mag.* **2012**, *76*, 227−253.

(6) King, H. E.; Mattner, D. C.; Plümper, O.; Geisler, T.; Putnis, A. Forming cohesive calcium oxalate layers on marble surfaces for stone conservation. *Cryst. Growth Des.* **2014**, *14*, 3910−3917.

(7) Jroundi, F.; Gonzalez-Muñoz, M. T.; Garcia-Bueno, A.; Rodriguez-Navarro, C. Consolidation of archaeological gypsum plaster by bacterial biomineralization of calcium carbonate. *Acta Biomater.* **2014**, *10*, 3844−3854.

(8) Ruiz-Agudo, C.; Álvarez-Lloret, P.; Di Lorenzo, F.; Gebauer, D.; Putnis, C. V. Baryte cohesive layers formed on a (010) gypsum surface by a pseudomorphic replacement. *Eur. J. Mineral.* **2019**, *31*, 289−299.

(9) Burgos-Cara, A.; Putnis, C. V.; Ortega-Huertas, M.; Ruiz-Agudo, E. Influence of pH and citrate on the formation of oxalate layers on calcite revealed by in situ nanoscale imaging. *CrystEngComm* **2017**, *19*, 3420−3429.

(10) Burgos-Cara, A.; Ruiz-Agudo, E.; Rodriguez-Navarro, C. Effectiveness of oxalic acid treatments for the protection of marble surfaces. *Mater. Des.* **2017**, *115*, 82−92.

(11) Prieto, M.; Cubillas, P.; Fernández-Gonzalez, Á. Uptake of dissolved Cd by biogenic and abiogenic aragonite: A comparison with sorption onto calcite. *Geochim. Cosmochim. Acta* **2003**, *67*, 3859−3869.

(12) Álvarez-Lloret, P.; Rodríguez-Navarro, A.; Falini, G.; Fermani, S.; Ortega-Huertas, M. Crystallographic control of the hydrothermal conversion of calcitic sea urchin spine (Paracentrotus lividus) into Apatite. *Cryst. Growth Des.* **2010**, *10*, 5227−5232.

(13) Forjanes, P.; Gómez-Barreiro, J.; Morales, J.; Astilleros, J. M.; Fernández-Díaz, L. Epitactic growth of celestite on anhydrite: Substrate induced twinning and morphological evolution of aggregates. *CrystEngComm* **2020**, *22*, 5743−5759.

(14) Perdikouri, C.; Kasioptas, A.; Geisler, T.; Schmidt, B. C.; Putnis, A. Experimental study of the aragonite to calcite transition in aqueous solution. *Geochim. Cosmochim. Acta* **2011**, *75*, 6211−6224.

(15) Perdikouri, C.; Piazolo, S.; Kasioptas, A.; Schmidt, B. C.; Putnis, A. Hydrothermal replacement of aragonite by calcite: Interplay between replacement, fracturing and growth. *Eur. J. Mineral.* **2013**, *25*, 123−136.

(16) Chen, L.; Yang, G. Epitaxial growth and cracking mechanisms of thermally sprayed ceramic splats. *J. Therm. Spray Technol.* **2018**, *27*, 255−268.

(17) De Villiers, J. P. R. Crystal structures of aragonite, strontianite, and witherite. *Am. Mineral.* **1971**, *56*, 758−767.

(18) Markgraf, S. A.; Reeder, R. J. High-temperature structure refinements of calcite and magnesite. *Am. Mineral.* **1985**, *70*, 590−600.

(19) Chang, L. L., Howie, R. A., Zussman, J.Nonsilicates: Sulfates, carbonates, phosphates and halides. *Rock Forming Minerals*; Longman, 1996.

(20) Putnis, A.*An Introduction to Mineral Sciences*; Cambridge University Press, 1992.

(21) Casella, L. A.; He, S.; Griesshaber, E.; Fernández-Díaz, L.; Greiner, M.; Harper, E. M.; Jackson, D. J.; Ziegler, A.; Mavromatis, V.; Dietzel, M.; Eisenhauer, A.; Veintemillas-Verdaguer, S.; Brand, U.; Schmahl, W. W. Hydrothermal alteration of aragonitic biocarbonates: Assessment of micro- and nanostructural dissolution−reprecipitation and constraints of diagenetic overprint from quantitative statistical grain-area analysis. *Biogeosciences* **2018**, *15*, 7451−7484.

(22) Forjanes, P.; Roda, M. S.; Greiner, M.; Griesshaber, E.; Lagos, N. A.; Veintemillas-Verdaguer, S.; Astilleros, J. M.; Fernández-Díaz, L.; Schmahl, W. W. Experimental burial diagenesis of aragonitic biocarbonates: from organic matter loss to abiogenic calcite formation. *Biogeosciences* **2022**, *19*, 3791−3823.

(23) Rodríguez-Carvajal, J. Recent advances in magnetic structure determination by neutron powder diffraction. *Phys. B* **1993**, *192*, 55−69.

(24) Rodriguez-Navarro, A. B. XRD2DScan: New software for polycrystalline materials characterization using two-dimensional X-ray diffraction. *J. Appl. Crystallogr.* **2006**, *39*, 905−909.

(25) Paquette, J.; Reeder, R. J. Relationship between surface structure, growth mechanism, and trace element incorporation in calcite. *Geochim. Cosmochim. Acta* **1995**, *59*, 735−749.
(26) Ruiz-Agudo, E.; Kudłacz, K.; Putnis, C. V.; Putnis, A.; Rodriguez-Navarro, C. Dissolution and carbonation of portlandite [$Ca(OH)_2$] single crystals. *Environ. Sci. Technol.* **2013**, *47*, 11342−11349.
(27) Jordan, G.; Higgins, S. R.; Eggleston, C. M.; Knauss, K. G.; Schmahl, W. W. Dissolution kinetics of magnesite in acidic aqueous solution, a hydrothermal atomic force microscopy (HAFM) study: Step orientation and kink dynamics. *Geochim. Cosmochim. Acta* **2001**, *65*, 4257−4266.
(28) Pérez-Garrido, C.; Astilleros, J. M.; Fernández-Díaz, L.; Prieto, M. In situ AFM study of the interaction between calcite {1014} surfaces and supersaturated Mn^{2+}−CO_3^{2-} aqueous solutions. *J. Cryst. Growth* **2009**, *311*, 4730−4739.
(29) Putnis, A.; Prieto, M.; Fernandez-Diaz, L. Fluid supersaturation and crystallization in porous media. *Geol. Mag.* **1995**, *132*, 1−13.
(30) Putnis, A. Mineral Replacement Reactions. *Rev. Mineral. Geochem.* **2009**, *70*, 87−124.
(31) Franke, W.; Hofer, A.; Jelinski, B.; Lenk, K. The morphology of witherite and strontianite grown in Silica Gel, by slow precipitation and on hydrothermal conditions. *Cryst. Res. Technol.* **1984**, *19*, 1565−1569.
(32) Dam, B.; Bennema, P.; Van Enckevort, W. J. P. The mechanism of tapering on KDP-type crystals. *J. Cryst. Growth* **1986**, *74*, 118−128.
(33) Lu, T.; Yallee, R. B.; Ong, C. K.; Sunagawa, I. Formation mechanism of tapering of crystals: a comparative study between potassium dihydrogen phosphate crystals and natural quartz crystals. *J. Cryst. Growth* **1995**, *151*, 342−347.
(34) Veintemillas-Verdaguer, S.; Rodríguez-Clemente, R. Crystal growth of KDP from boiling solutions in the presence of impurities. *J. Cryst. Growth* **1986**, *79*, 198−204.
(35) Wu, W.; Ma, Y.; Xing, Y.; Zhang, Y.; Yang, H.; Luo, Q.; Wang, J.; Li, B.; Qi, L. Ca-Doped strontianite−calcite hybrid micropillar arrays formed via oriented dissolution and heteroepitaxial growth on calcite. *Cryst. Growth Des.* **2015**, *15*, 2156−2164.
(36) Wu, W.; Zhang, Z.; Li, B.; Ma, Y. Epitaxial growth of single-crystalline barium carbonate microcone arrays on (104) face of calcite. *Acta Phys.-Chim. Sin.* **2015**, *31*, 189−198.
(37) Van Der Merwe, J. H. The role of lattice misfit in epitaxy. *Crit. Rev. Solid State Mater. Sci.* **1978**, *7*, 209−231.
(38) Rodríguez-Blanco, J. D.; Jiménez, A.; Prieto, M. Oriented overgrowth of pharmacolite ($CaHAsO_4{\cdot}2H_2O$) on gypsum ($CaSO_4{\cdot}2H_2O$). *Cryst. Growth Des.* **2007**, *7*, 2756−2763.
(39) Chernov, A. A.Nucleation and epitaxy. *Modern Crystallography III: Crystal Growth*; En Chernov, A. A., Ed.; Springer, 1984; pp 48−103.
(40) Pérez-Garrido, C.; Fernández-Díaz, L.; Pina, C. M.; Prieto, M. In situ AFM observations of the interaction between calcite (1014) surfaces and Cd-bearing aqueous solutions. *Surf. Sci.* **2007**, *601*, 5499−5509.
(41) Riechers, S. L.; Kerisit, S. N. Anisotropic growth of otavite on calcite: Implications for heteroepitaxial growth mechanisms. *Cryst. Growth Des.* **2018**, *18*, 159−170.
(42) Di Lorenzo, F.; Ruiz-Agudo, C.; Churakov, S. V. The key effects of polymorphism during PbII uptake by calcite and aragonite. *CrystEngComm* **2019**, *21*, 6145−6155.
(43) Di Lorenzo, F.; Cametti, G.; Vanhecke, D.; Churakov, S. V. The role of interfaces in controlling Pb^{2+} removal by calcium Carbonate minerals. *Cryst. Growth Des.* **2020**, *20*, 6157−6169.
(44) Shtukenberg, A. G.; Astilleros, J. M.; Putnis, A. Nanoscale observations of the epitaxial growth of hashemite on barite (001). *Surf. Sci.* **2005**, *590*, 212−223.
(45) Xu, M.; Riechers, S. L.; Ilton, E. S.; Du, Y.; Kovarik, L.; Varga, T.; Arey, B. W.; Qafoku, O.; Kerisit, S. Manganese-calcium intermixing facilitates heteroepitaxial growth at the 1014 calcite-water interface. *Chem. Geol.* **2017**, *470*, 152−163.
(46) Roncal-Herrero, T.; Astilleros, J. M.; Bots, P.; Rodríguez-Blanco, J. D.; Prieto, M.; Benning, L. G.; Fernández-Díaz, L. Reaction pathways and textural aspects of the replacement of anhydrite by calcite at 25 °C. *Am. Mineral.* **2017**, *102*, 1270−1278.
(47) Pedrosa, E. T.; Putnis, C. V.; Renard, F.; Burgos-Cara, A.; Laurich, B.; Putnis, A. Porosity generated during the fluid-mediated replacement of calcite by fluorite. *CrystEngComm* **2016**, *18*, 6867−6874.
(48) Forjanes, P.; Astilleros, J. M.; Fernández-Díaz, L. The formation of barite and celestite through the replacement of gypsum. *Minerals* **2020**, *10*, 189.
(49) Beaudoin, N.; Hamilton, A.; Koehn, D.; Shipton, Z. K.; Kelka, U. Reaction-induced porosity fingering: Replacement dynamic and porosity evolution in the KBr-KCl system. *Geochim. Cosmochim. Acta* **2018**, *232*, 163−180.
(50) Mayorga, I. C.; Astilleros, J. M.; Fernández-Díaz, L.; Morales, J.; Prieto, M.; Roncal-Herrero, T.; Benning, L. G. Epitactic overgrowths of calcite ($CaCO_3$) on anhydrite ($CaSO_4$) cleavage surfaces. *Cryst. Growth Des.* **2018**, *18*, 1666−1675.
(51) Szucs, A. M.; Stavropoulou, A.; O'Donnell, C.; Davis, S.; Rodriguez-Blanco, J. D. Reaction pathways toward the formation of bastnäsite: Replacement of calcite by Rare Earth carbonates. *Cryst. Growth Des.* **2021**, *21*, 512−527.
(52) Yuan, K.; Lee, S. S.; De Andrade, V.; Sturchio, N. C.; Fenter, P. Replacement of calcite ($CaCO_3$) by cerussite ($PbCO_3$). *Environ. Sci. Technol.* **2016**, *50*, 12984−12991.
(53) Yuan, K.; De Andrade, V.; Feng, Z.; Sturchio, N. C.; Lee, S. S.; Fenter, P. Pb^{2+}−calcite interactions under far-from-equilibrium conditions: Formation of micropyramids and pseudomorphic growth of cerussite. *J. Phys. Chem. C* **2018**, *122*, 2238−2247.
(54) Kim, Y.; Abdilla, B.; Yuan, K.; De Andrade, V.; Sturchio, N. C.; Lee, S. S.; Fenter, P. Replacement of calcium carbonate polymorphs by cerussite. *ACS Earth Space Chem.* **2021**, *5*, 2433−2441.
(55) Putnis, C. V.; Geisler, T.; Schmid-Beurmann, P.; Stephan, T.; Giampaolo, C. An experimental study of the replacement of leucite by analcime. *Am. Mineral.* **2007**, *92*, 19−26.
(56) Jamtveit, B.; Putnis, C. V.; Malthe-Sørenssen, A. Reaction induced fracturing during replacement processes. *Contrib. Mineral. Petrol.* **2009**, *157*, 127−133.
(57) Lafay, R.; Montes-Hernandez, G.; Renard, F.; Vonlanthen, P. Intracrystalline reaction-induced cracking in olivine evidenced by hydration and carbonation experiments. *Minerals* **2018**, *8*, 412.
(58) Gillet, P.; Gérard, Y.; Willaime, C. The calcite-aragonite transition: Mechanism and microstructures induced by the transformation stresses and strain. *Bull. Mineral.* **1987**, *110*, 481−496.
(59) Kondo, Y. Prediction of fatigue crack initiation life based on pit growth. *Corrosion* **1989**, *45*, 7−11.
(60) Plümper, O.; Røyne, A.; Magrasó, A.; Jamtveit, B. The interface-scale mechanism of reaction-induced fracturing during serpentinization. *Geology* **2012**, *40*, 1103−1106.
(61) Monasterio-Guillot, L.; Fernandez-Martinez, A.; Ruiz-Agudo, E.; Rodriguez-Navarro, C. Carbonation of calcium-magnesium pyroxenes: Physical-chemical controls and effects of reaction-driven fracturing. *Geochim. Cosmochim. Acta* **2021**, *304*, 258−280.

https://doi.org/10.1021/acs.cgd.2c00383
Cryst. Growth Des. 2022, 22, 6418−6428